Volume 49
Number 37
7 October 2025
Pages 15985–16466

NJC

New Journal of Chemistry

A journal for new directions in chemistry

rsc.li/njc

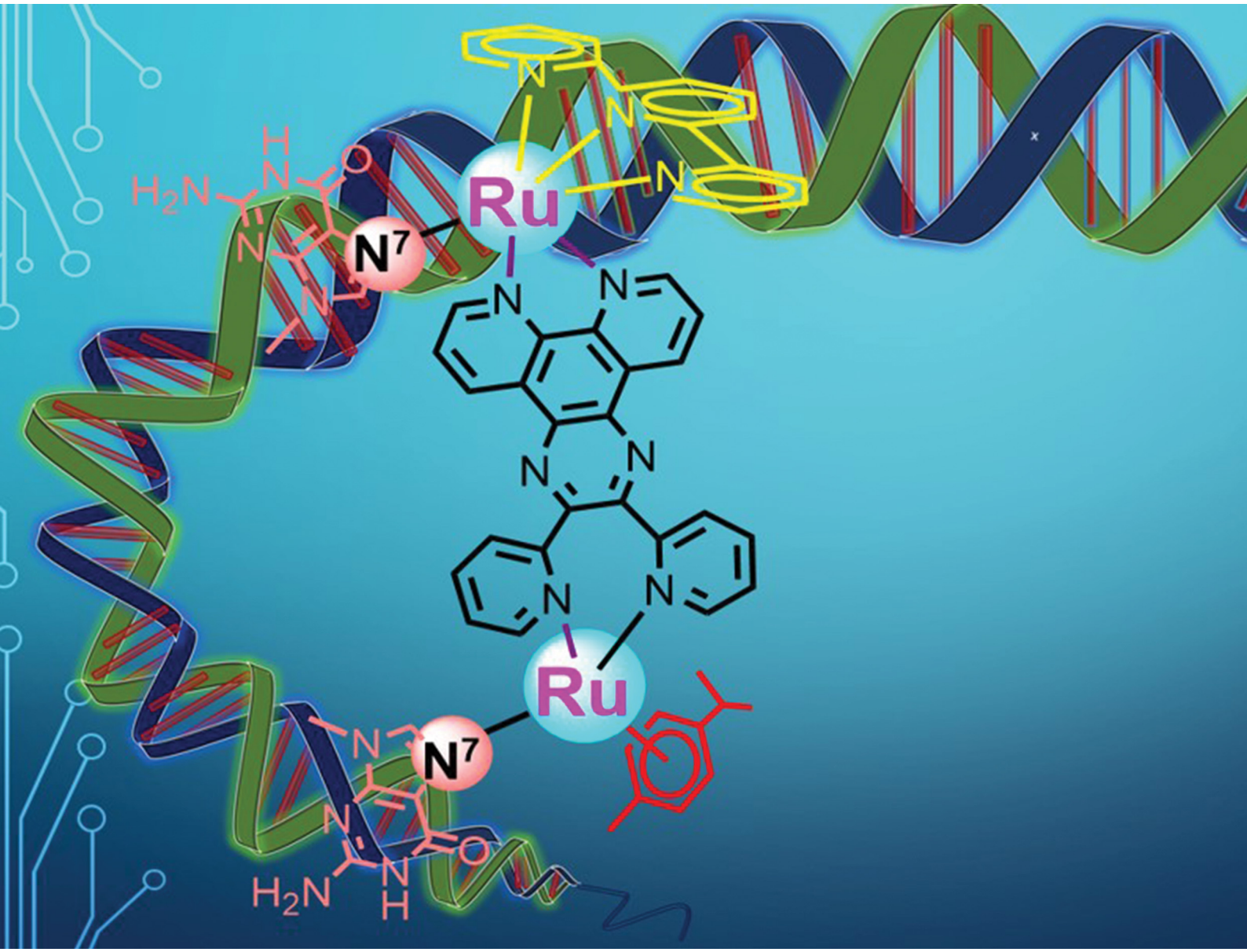

ISSN 1144-0546

ROYAL SOCIETY OF CHEMISTRY

PAPER

Anwesha Mohanty and Srikanta Patra
Synthesis, characterization, computational and DNA interaction studies of mono- and dinuclear Ru(II) complexes containing terpyridine and *p*-cymene ligands

cnrs

NJC

ROYAL SOCIETY OF CHEMISTRY

PAPER

View Article Online
View Journal | View Issue

Cite this: *New J. Chem.*, 2025, **49**, 15999

Synthesis, characterization, computational and DNA interaction studies of mono- and dinuclear Ru(II) complexes containing terpyridine and *p*-cymene ligands†

Anwesha Mohanty and Srikanta Patra *

Herein, we present the development of three heteroleptic ruthenium complexes {two mononuclear [(tpy)Ru(phpy)Cl]ClO_4; [**1**], [(*p*-cym)Ru(phpy)Cl]ClO_4; [**2**], and a dinuclear [(tpy)RuCl(μ-phpy)Ru(*p*-cym)Cl]$(ClO_4)_2$; [**3**]} using terpyridine (tpy), *p*-cymene (*p*-cym) and semi-flexible phenanthroline-pyrazine-based (phpy) ligands. The formation of 1–**3** was confirmed by HRMS, and ^{1}H and ^{13}C NMR spectroscopy. Furthermore, ^{1}H–^{1}H correlation spectroscopy was also done to support the possible assignment of the dinuclear **3**. The redox and optical properties of the complexes were studied using cyclic voltammetry and UV-Vis spectroscopy. The DNA binding interaction study of the complexes was investigated utilizing the UV-Vis absorption titration and EB-displacement assay employing calf-thymus DNA (ct-DNA). The complexes display binding constants (K_b) of 5.5×10^3 M^{-1}, 5.7×10^3 M^{-1} and 8.2×10^3 M^{-1} and the Stern–Volmer constants (K_{SV}) 2.7×10^5 M^{-1}, 1.3×10^4 M^{-1}, and 1.1×10^5 M^{-1} for **1**, **2**, and **3**, respectively. The observed K_b and K_{SV} values are found to be governed by the rigidity, planarity and labile Cl^- functionality present in the complexes. The results demonstrate a moderately strong mixed mode of interaction between the complexes and CT-DNA and suggest their potential to act as good anticancer agents.

Received 22nd May 2025,
Accepted 26th June 2025

DOI: 10.1039/d5nj02167g

rsc.li/njc

1. Introduction

Ruthenium(II)-based complexes have been known in the literature for decades due to their appealing features like facile synthetic procedure, interesting redox and photophysical properties, exciting chemical[1–4] and biological activity,[5–9] and applications in different fields of science and technology. The properties can be conveniently fine-tuned by facile modification of the ligand frameworks *via* the introduction of donors and functionality making them suitable for desired applications.[10,11] Among various ligands, terpyridyl and half-sandwiched *p*-cymene (*p*-cym) are attractive for facile incorporation of varying functionalities in their framework and ability to form stable complexes. In both the half-sandwiched {(*p*-cym)RuCl} and {(tpy)RuCl} frameworks, three coordination sites are occupied by *p*-cym or tpy ligands offering a specific geometry. The other two coordination sites can be occupied by a bidentate ligand. The sixth coordination site is generally linked with a labile Cl^- group, which can be easily replaced by a desired ligand (Fig. 1). Considering this, a plethora of mononuclear complexes with {(*p*-cym)RuCl} and {(tpy)RuCl} frameworks have been developed and studied. The {(*p*-cym)RuCl} based complexes exhibited excellent catalytic activity for various important organic transformations[12–15] and agents for anticancer and antibacterial activity.[9,16,17] On the other hand, in addition to their excellent biological activity,[18–21] {(tpy)RuCl} based complexes also display interesting optoelectronic properties[1,20,22–24] and application in various areas like water splitting,[25,26] sensing,[27–29] light harvesting units,[23,30] charge storage devices,[31–33] photosensitizers,[4,24,34] *etc.* Although a great number of mononuclear complexes of {(*p*-cym)RuCl} and {(tpy)RuCl} frameworks have been developed and studied, dinuclear complexes having both the aforesaid frameworks, have not yet been disclosed. It would be worthy to explore dinuclear ruthenium complexes having different ancillary ligand frameworks and study the effect of bridging ligand and its conjugation on the electronic communication between the metal centres and two labile chloride ligands of different environments. Recently, our group has developed a semi-flexible phenanthroline-pyrazine-based 2,3-di(pyridin-2-yl)pyrazino[2,3-*f*][1,10] phenanthroline (**phpy**) ligand which acts as an excellent bridging ligand for homo- and heterodimetallic systems.[35,36] Furthermore, because of its semi-flexible nature, the **phpy** ligand can show $N^{\wedge}N_{phen} \cap N^{\wedge}N_{pz}$ or $N^{\wedge}N_{phen} \cap N^{\wedge}N^{\wedge}C_{pz}$ binding mode.[35,36] Thus, it could be interesting to incorporate both

School of Basic Sciences, Indian Institute of Technology Bhubaneswar, Argul, Jatni, Odisha-752050, India. E-mail: srikanta@iitbbs.ac.in

† Electronic supplementary information (ESI) available. See DOI: https://doi.org/10.1039/d5nj02167g

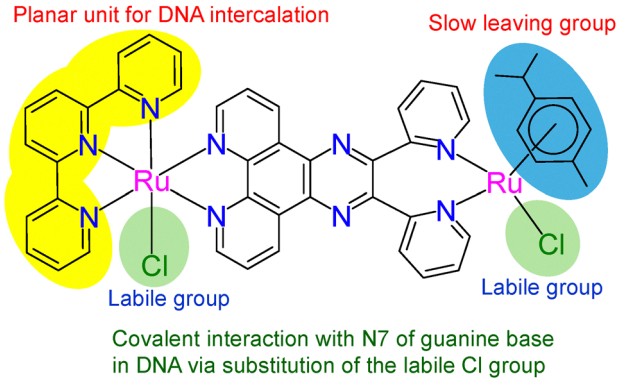

Fig. 1 General representation of the synthesised Ru(II) complex.

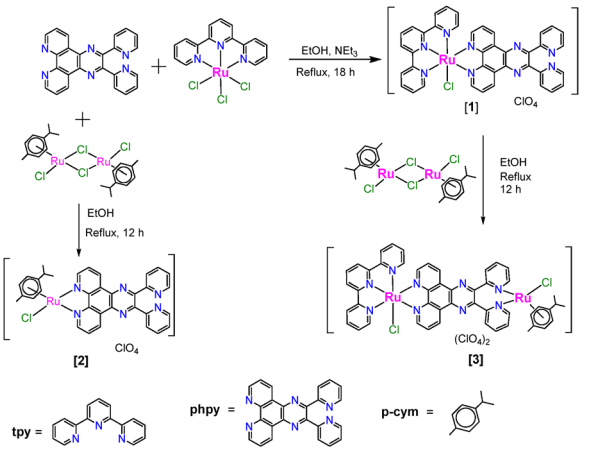

Scheme 1 Synthetic route for the preparation of **1**–**3**.

{(*p*-cym)RuCl} and {(tpy)RuCl} units in a single molecular framework through the **phpy** ligand and explore their properties (Fig. 1).

With this hypothesis, in the present contribution, we report the synthesis of two mononuclear complexes [(tpy)RuCl(phpy)]ClO_4 (**1**) and [(*p*-cym)RuCl(phpy)]ClO_4 (**2**), and a dinuclear complex [(*p*-cym)RuCl(μ-phpy)RuCl(tpy)]$(ClO_4)_2$ (**3**) [*p*-cym = *p*-cymene, tpy = 2,2′:6′,2″-terpyridine] and their electrochemical, spectroscopic, computational and DNA binding studies. The formation of the complexes and their characterization were carried out by various analytical techniques. The interaction of the complexes with CT-DNA and the effect of *p*-cymene and tpy ligands were investigated by UV-Vis and fluorescence spectroscopic techniques.

2. Results and discussion

2.1. Synthesis and spectral aspects

The **phpy** ligand was prepared *via* the condensation reaction between 5,6-diamino-1,10-phenanthroline with commercially available 2,2′-pyridil.[35,36] Mononuclear **1** and **2** were obtained by reacting **phpy** ligand and appropriate ratios of respective precursors in refluxing ethanol under a dinitrogen environment (Scheme 1), followed by salt metathesis and repeated precipitation/chromatographic separation (Experimental section). The dinuclear **3** was prepared by reacting mononuclear **1** and dimeric [*p*-cym)RuCl(μ-Cl)]$_2$ precursor in a 2 : 1 ratio under the aforesaid reaction conditions and purified by repeated precipitation (Scheme 1).

The high-resolution positive ion ESI mass spectra of the complexes (Fig. 2) display molecular ion peaks centred at 756.0961 (calcd 756.0965) for [**1**-ClO_4]$^+$ and 657.1086 (calcd 657.1107) for [**2**-ClO_4]$^+$. Interestingly, along with the molecular ion peak at 1126.0202 (calcd 1126.0277) corresponding to [**3**-ClO_4]$^+$, complex **3** also displays a base peak corresponding to {[**3**-2ClO_4]$^{2+}$}/2 at 513.5376 (calcd 513.5396). The corresponding simulated HRMS pattern of the complexes also nicely fits with those of the experimentally observed spectra, which supports their formation and the existence of the entire molecular framework.

The ^{1}H NMR spectra of **1**, **2** and **3** in DMSO-d_6 exhibit 25, 18 and 29 aromatic proton signals in the region 4.5–10.5 ppm, confirming the presence of the **phpy** ligand, [(tpy)Ru] and [(*p*-cym)Ru] fragments in the respective complexes (Fig. S1, ESI†). Intense singlets at 0–2.0 ppm due to CH_3 protons further support the existence of the [(*p*-cym)Ru] fragment in the complexes **2** and **3**. The ^{13}C NMR spectra of the complexes also display the required number of carbon signals, which further supports their formation (Fig. S2, ESI†).

Furthermore, the ^{1}H–^{1}H COSY spectral study of dinuclear **3** was carried out. The best possible correlation with the neighbouring protons further supports its assignment (Fig. 3).

A DFT-based computational approach in the gas phase using the B3LYP functional was undertaken to obtain the optimized geometry and analyse the photophysical properties of the complexes. The optimized geometry and SCF energy of the ground state (S_0) of the complexes (**1**$^+$–**3**$^{2+}$) are shown in Fig. 4 and Fig. S3 (ESI†). The optimized bond parameters are depicted in Tables S1–S3 (ESI†). From the optimized geometry, it is observed that the HOMO of **1**$^+$ is mainly localized on the Ru unit (55%) and chloride ligand (31%), whereas the LUMO resides at the terpyridine unit (90%) (Fig. S4 and Table S4, ESI†). However, for the half-sandwiched **2**$^+$, both the HOMO (97%) and LUMO (93%) are localized on the **phpy** ligand (Fig. S5 and Table S5, ESI†). Interestingly, for dinuclear **3**$^{2+}$, the HOMO is primarily localized on the Ru centre (53%) and Cl^- (33%) of [(tpy)RuCl] similar to HOMO of **1**; however, the LUMO resides majorly on the **phpy** ligand (75%) with slight contribution of the Ru centre (13%) and *p*-cym ligand (9%) of the[(*p*-cym)RuCl] unit (Fig. 4, and Table S6, ESI†). The HOMO–LUMO energy gap is significantly higher (2.932 eV for **1**$^+$ and 3.461 eV for **2**$^+$) compared to the dinuclear **3**$^{2+}$ 2.258 eV.

The electrochemical characteristics of the complexes were investigated in acetonitrile using a glassy carbon working electrode, Pt wire counter electrode, and Ag/AgCl reference electrode (Fig. 5a). The mononuclear complexes exhibit one quasi-reversible one-electron redox couple ($E_{1/2}$ = 0.85 V) for **1** and an irreversible peak at 1.65 V for **2** corresponding to Ru^{II}/Ru^{III} oxidation processes.[35,37–39] The dinuclear **3** exhibits

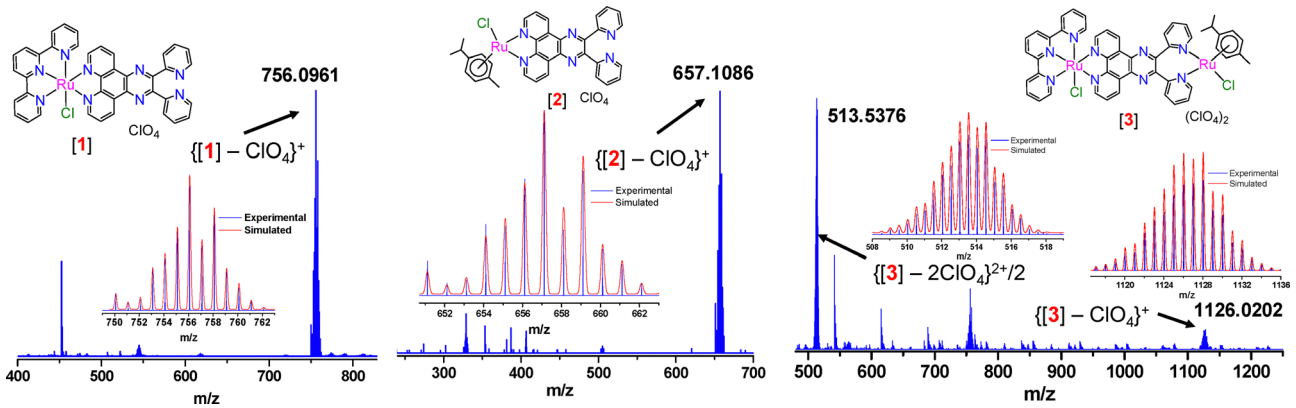

Fig. 2 Molecular structures of the complexes **1–3** and their corresponding HRMS spectra recorded in CH_3OH. The inset shows the isotopic distribution pattern of the molecular ion peaks.

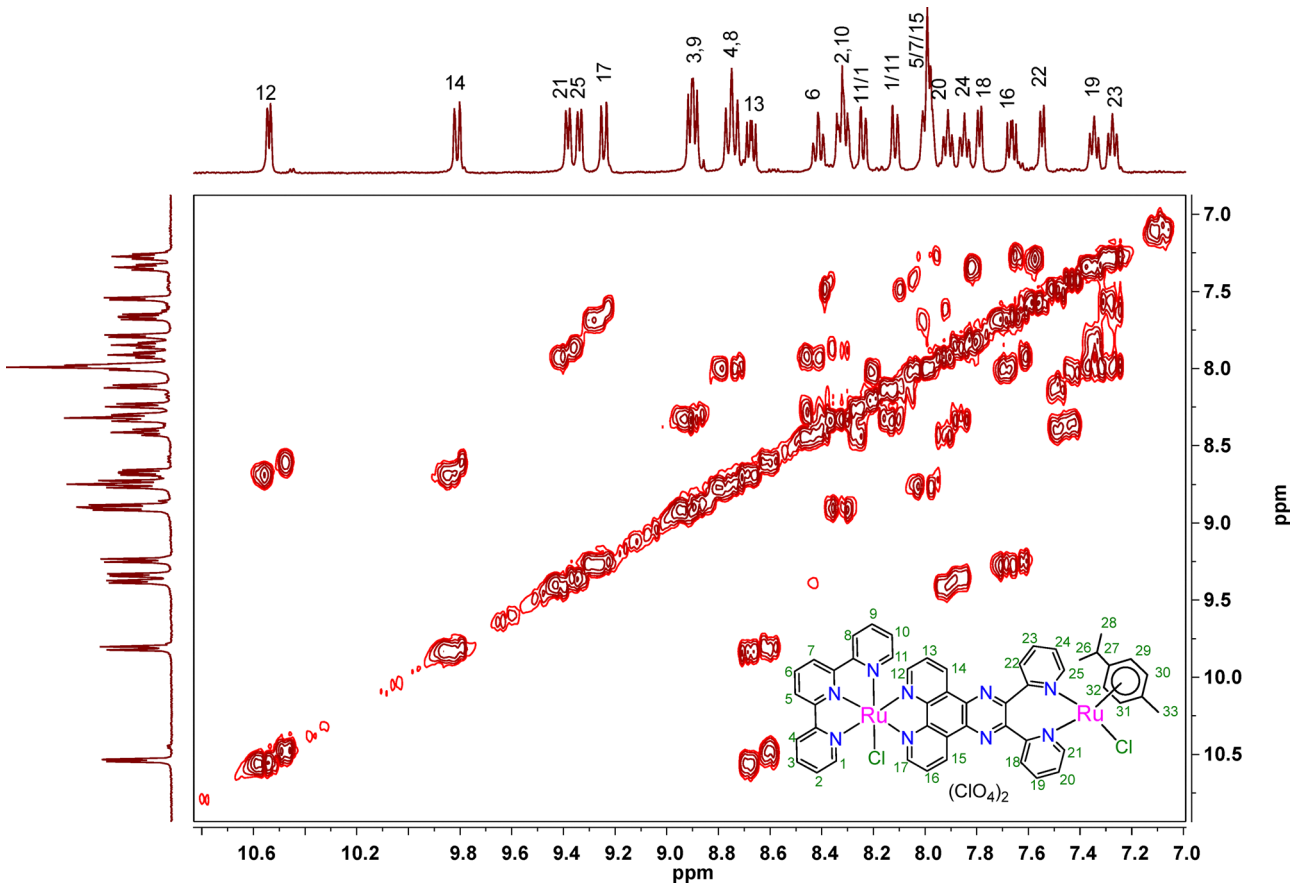

Fig. 3 $^1H–^1H$ COSY NMR spectrum of the complex **3** in $(CD_3)_2SO$.

two quasi-reversible Ru^{II}/Ru^{III} oxidative couples at $E_{1/2}$ = 0.85 V for the [(tpy)RuCl] side and 1.84 V corresponding to the [(*p*-cym)RuCl] framework, which is consistent with the reported literature values.[37,40] An additional irreversible oxidative signal is also observed at ~2.01 V and 1.98 V for **2** and **3**, respectively. This could be due to the further oxidation of Ru^{III}/Ru^{IV} of the [(*p*-cym)RuCl] framework.[35] Interestingly, a 0.19 V positive shift of Ru^{II}/Ru^{III} (*p*-cym) oxidation potential in dinuclear **3**, indicates good communication between the two ruthenium centres through the phpy bridge. Additionally, ligand-based reductions were also observed at the negative end of the cyclic voltammogram, possibly attributed to the reduction of the pyrazine-unit (~ −0.78 V) and phenanthroline unit of phpy, and terpyridine ligands at more −ve potential.[35,36]

The absorption spectra of the complexes were recorded in acetonitrile solvent at room temperature (Fig. 5b and Table 1).

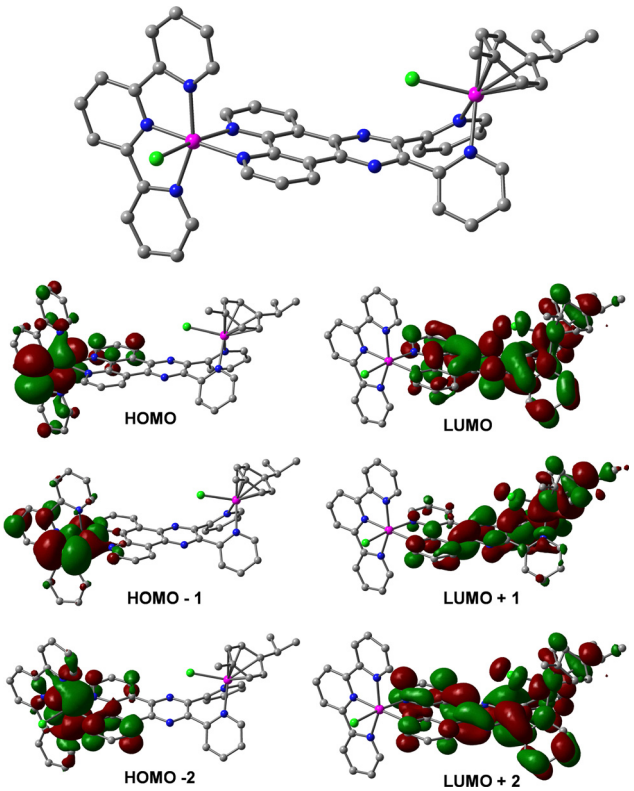

Fig. 4 DFT optimized geometry and pictorial representation of the Kohn–Sham frontier orbitals of $\mathbf{3}^{2+}$ in the gas phase.

The mononuclear **1** and dinuclear **3** exhibit low energy bands with λ_{max} at 510 nm, which is the signature of ruthenium terpyridyl-based complexes.[40–42] The intensity of dinuclear **3** has significantly dropped as compared to mononuclear **1** after incorporation of the [(*p*-cym)RuCl] fragment in the molecular framework. This low-energy band is absent for mononuclear **2**. This observation suggests that the aforesaid band could be Ru $\rightarrow \pi^*_{tpy}$ metal to ligand charge transfer (MLCT) transition.[41,42] The TDDFT results also agree with the above assignment (Tables S7–S9, ESI†). In the high-energy ultraviolet region (350 nm and 280 nm), all the complexes display intense phpy or tpy-based ligand-to-ligand charge transfer (ILCT/LLCT; π–π*) transitions, which is in line with the TDDFT analysis (Tables S7–S9, ESI†). An additional high energy band is observed at 315 nm for **1** and **3**, which could be due to the intra ligand $\pi_{tpy} \rightarrow \pi^*_{phpy}$ charge transfer transition or *vice versa*.[28,38,40]

The emission spectra of the complexes **1–3** were recorded in phosphate buffer (PB, pH 7.4) at room temperature. It was observed that complexes **1** and **3** are non-fluorescent upon excitation at 510 nm (Fig. S6, ESI†). However, complex **2** exhibits moderately good emission behavior with emission maxima at 390 nm with quantum yield of 0.0067 against standard $[Ru(bpy)_3]^{2+}$, upon excitation at 360 nm (Fig. S6, ESI†). This type of emission behavior was also observed with structurally similar complexes.[43]

2.2. Electronic absorption titration studies

Polypyridyl complexes of [(tpy)RuCl] and [(*p*-cym)RuCl] are known for their interaction with biomolecules.[6,19,27,38] To understand the possible binding mode of the complexes with CT-DNA, UV-Vis spectral studies have been conducted by measuring the changes in absorption upon aliquot addition of CT-DNA (0–100 μM) to a fixed amount of complexes (34 μM).[44] Usually, intercalation of the complexes with DNA base pairs causes hypochromic along with/without blue/red shifts, while non-intercalative/external electrostatic binding is followed by hyperchromic shift.[21,45]

The magnitude of hypochromism gives an idea about the strength of intercalative binding mode of interaction. UV-Vis

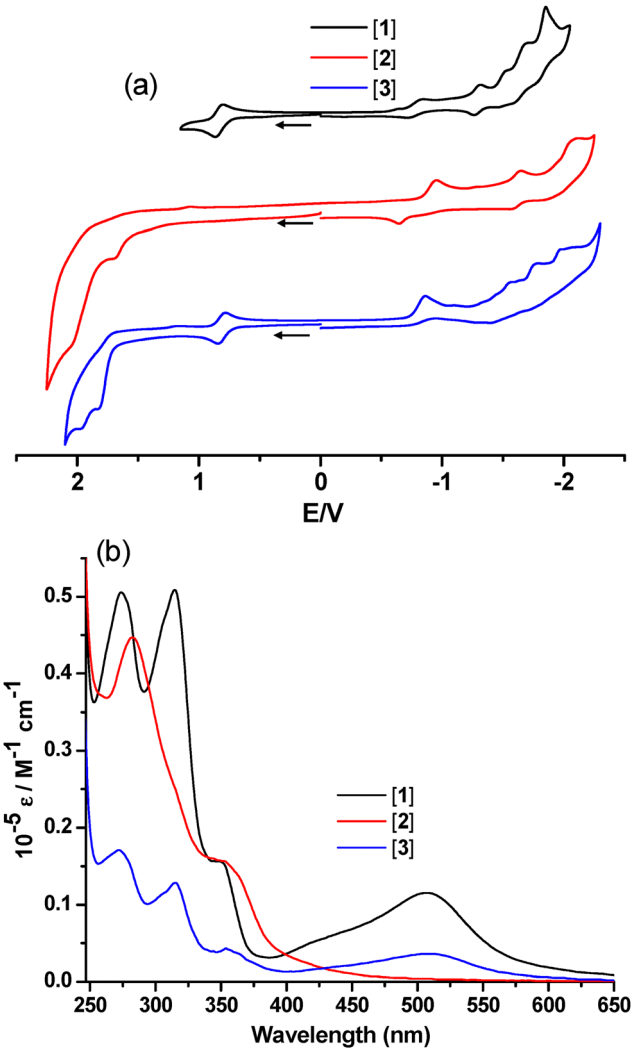

Fig. 5 (a) Cyclic voltammograms and (b) UV-Vis spectra of the complexes **1–3** recorded in CH_3CN. The voltammograms were recorded against the Ag/AgCl reference electrode and glassy carbon working electrode, and the potentials were adjusted against Fc/Fc^+.

Table 1 UV-Vis spectral data of the complexes **1–3** recorded in CH_3CN

[Complex]	$\varepsilon \times 10^4$ (M^{-1} cm^{-1}) (λ_{max}, nm)
[**1**]	1.16 (509), 1.55 (352), 5.09 (315), 5.07 (274)
[**2**]	1.48 (359), 4.48 (282)
[**3**]	0.38 (509), 0.42 (357), 1.28 (315), 1.73 (272)

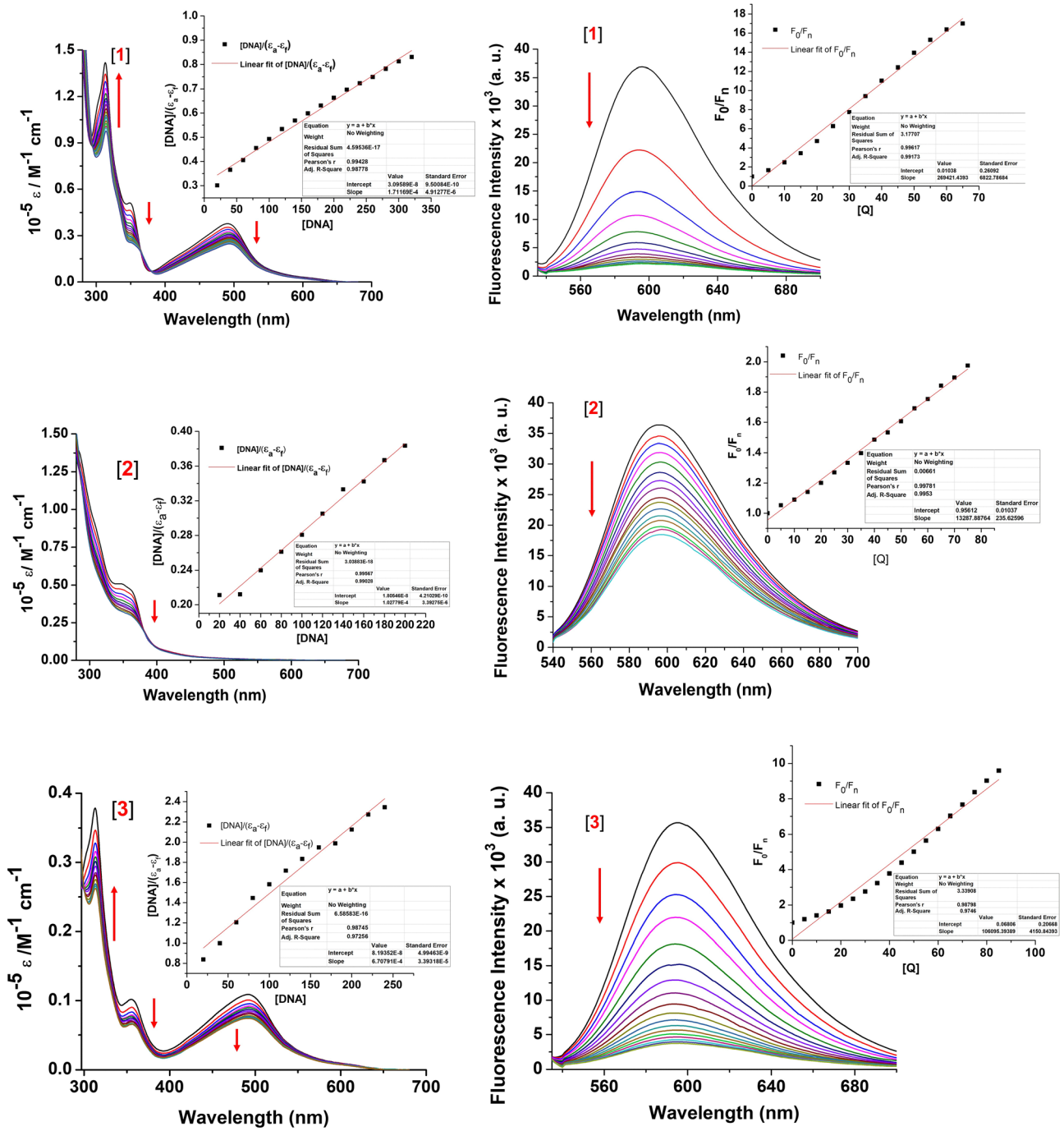

Fig. 6 UV-Vis titration (left) and EB displacement (right) assay of complexes **1–3** in a phosphate buffer (10 mM, pH 7.4). Absorption spectra were recorded upon the addition of CT-DNA. Conditions: [complex] = 34 μM, [DNA] = 0–100 μM. Emission spectra (bottom) were recorded upon addition of complexes to a solution of EB–CT-DNA adduct. Conditions: [DNA] = 20 μM, [complex] = 0–100 μM. The arrow shows the decrease in absorption/emission intensity. The inset shows the binding isotherm.

titration spectra for 1–3 with CT-DNA are depicted in Fig. 6. From the absorption titration curves, it is clear that the band for **1** present at 492 nm exhibited hypochromism (ε, 1.1×10^4–7.3×10^3 M^{-1} cm^{-1}). However, the band at 313 nm displayed hyperchromism with a slight red shift of 7 nm. Similarly, gradual addition of CT-DNA (10 μM) to a solution of **2** and **3** led to the low energy bands at 355 nm and 492 nm displaying hypochromism without any shift (ε, 1.4×10^4–9.2×10^3 M^{-1} cm^{-1} for **2** at 355 nm and ε, 3.2×10^3–2.2×10^3 M^{-1} cm^{-1}, 492 nm for **3**). These observed spectral changes might be due to the interaction of the complexes with CT-DNA, leading to the formation of DNA–complex adduct *via* intercalative, groove binding and/or electrostatic interactions.[21,46]

To investigate the magnitude of binding of metal complexes towards CT-DNA, intrinsic binding constants (K_b) were

calculated using Bard's equation based on the McGhee–von Hippel (MvH) model.

$$\frac{[DNA]}{|\varepsilon_a - \varepsilon_f|} = \frac{[DNA]}{|\varepsilon_b - \varepsilon_f|} + \frac{1}{K_b}\frac{1}{|\varepsilon_b - \varepsilon_f|} \quad (1)$$

where [DNA] represents the concentration of DNA in base pairs, ε_a is the apparent extinction coefficient enumerated as A_{obs}/[complex], and ε_f and ε_b stands for molar extinction coefficient for the complex in its free form and fully bound to CT-DNA. The values of slope and intercept were evaluated by $1/(\varepsilon_b - \varepsilon_f)$ and $1/K_b$ $(\varepsilon_b - \varepsilon_f)$ from the plot of $[DNA]/(\varepsilon_a - \varepsilon_f)$ *vs.* [DNA]. The calculated K_b values are found to be 5.5×10^3 M^{-1} for **1**, 5.7×10^3 M^{-1} for **2** and 8.2×10^3 M^{-1} for **3** indicating moderately strong interaction of the complexes with CT-DNA and are comparable to earlier reports.[44]

2.3. Ethidium bromide (EB) displacement studies

To get further insight into the interaction, nature of bonding, binding affinities, and binding constant of CT-DNA with complexes 1–**3**, ethidium bromide (EB) displacement studies have also been conducted. EB is known to be a weak emitter; however, it exhibits strong fluorescence when intercalated with CT-DNA.[6,10,44] The fluorescence intensity of the EB–CT-DNA adduct decreases upon displacement by the test complexes. The displacement of EB from the EB–CT-DNA adduct by complexes 1–**3** is shown in Fig. 6. It is seen from the figure that increasing the concentration of the complexes causes a moderate decrease in fluorescence intensity at 595 nm. This indicates the interaction of the complexes with CT-DNA *via* intercalation.[44] The magnitude of interaction of the complexes with CT-DNA has been assayed quantitatively by using the Stern–Volmer equation (eqn (2)).

$$\frac{F_0}{F} = 1 + K_{SV}[Q] \quad (2)$$

where F_0 and F are the fluorescence intensity of the EB–CT-DNA adduct before and after the addition of the complexes, K_{SV} is the Stern–Volmer constant, and [Q] is the concentration of the desired complex added. The K_{SV} values calculated from the slope of plot F_0/F *vs.* [Q] are 2.7×10^5 M^{-1}, 1.3×10^4 M^{-1}, and 1.1×10^5 M^{-1} for **1**, **2**, and **3**, respectively. The apparent binding constant has also been evaluated by using the Scatchard equation (eqn (3)).

$$K_{app} = K_{EB}[EB]/Q_{50\%} \quad (3)$$

where K_{app} is the apparent binding constant, K_{EB} is the binding constant of EB to CT DNA, and $[Q]_{50\%}$ is the concentration of complexes at 50% of the initial fluorescence intensity. The apparent binding constants of complexes 1–**3** are found to be 4.7×10^5 M^{-1}, 6.3×10^4 M^{-1} and 1.9×10^5 M^{-1}, respectively, indicating that **1** and **3** replace EB more efficiently than **2**, thereby reflecting their better intercalating ability.

Terpyridine ligands are known to interact through intercalation, whereas arene-ruthenium complexes are weak intercalators but interact covalently with N7 of guanine bases in DNA *via* substitution of the labile Cl unit.[29] Given that UV-Vis spectroscopy is sensitive to all modes of interaction between metal complexes and CT-DNA, complex **1** having planar terpyridyl and semi-flexible phenanthroline–pyrazine ligand frameworks, is expected to interact predominantly *via* intercalation.[21,46] In the case of complex **2**, the enhanced binding affinity observed in UV-Vis titration, may be attributed to direct coordination with DNA. Although complex **3** possesses planar ligand motifs similar to those in **1**, its ability to intercalate appears to be hindered due to the coordination of the [(*p*-cym)RuCl] fragment to the flexible site of the phpy moiety. This spatial constraint likely impedes effective DNA intercalation, which is reflected in its EB-displacement assay. However, the presence of the {(*p*-cym)RuCl} framework enables complex **3** to exhibit other modes of binding, thereby enhancing the overall binding efficiency, which is supported by the UV-Vis titration study. Apart from the aforesaid, the shape of the complexes and the adjustable features such as orientation of labile chloride ligands at [(tpy)RuCl] and/or [(*p*-cym)RuCl] fragments, presence of aromatic rings and their flexibility also have a significant influence on the mode of interaction with the DNA and observed binding constants.[10,11,45]

The binding constant values (K_b, K_{SV} and K_{app}) obtained from both UV-Vis and fluorescence spectroscopy indicates a moderately strong interaction of the complexes with CT-DNA and can be envisioned to exhibit good anticancer activity.

3. Conclusion

The present study offers the synthesis of three new heteroleptic Ru(II) complexes consisting of tpy, *p*-cym and semi-flexible **phpy** ligands. All the complexes were well characterized *via* different spectroscopic and analytical tools. The interaction of the complexes with CT-DNA was assayed using UV-vis and fluorescence spectroscopic techniques. The UV-Vis titration studies display the increasing order of overall binding affinity of the complexes as **1** < **2** < **3**, whereas the EB-displacement assay shows the order **2** < **3** < **1** due to better intercalating ability of **1** and **3**. Although the binding of the complexes is not as strong as classical intercalator ethidium bromide, the observed binding constants would be anticipated to show good biological activity. We believe that the present study offers a valuable insight to the community who are working on developing anticancer agents using terpyridine and *p*-cymene based ligand frameworks.

4. Experimental

4.1. Materials

All chemicals and solvents were reagent grade and used without further purification. Alumina gel (60–120 mesh) was employed for chromatography. HPLC-grade solvents were utilized for spectroscopic and electrochemical analyses. Highly pure water was obtained through a Milli Q water purification system. All the glasswares were thoroughly cleaned, rinsed with the required amount of double distilled water, and then dried in

a hot air oven. The metal complex syntheses were carried out under a dinitrogen atmosphere using a standard Schleck line.

The $[Ru(tpy)Cl_3]$,[47] $[(p\text{-cym})Ru(\mu\text{-}Cl)Cl]_2$[48] precursors and pyrazine-based bridging ligand (phpy)[36] were prepared as per reported methods.

4.2. Physical measurements

The solution conductivity of the complexes in CH_3CN (0.5 mM) was measured using an OAKton PC 2700 Conductivity Bridge. Electrospray ionization (ESI) mass spectra were recorded using a Thermo Fisher Scientific Q Exactive Plus Orbitrap mass spectrometer in CH_3OH solvent. ^1H and ^{13}C NMR spectral data were collected in $(CD_3)_2SO$ solvent at 298 K on a Bruker Avance III 400 spectrometer. UV-Vis spectra were obtained with a Shimadzu UV-1800 spectrophotometer, maintaining a constant concentration of all complexes at 10 μM. Fluorescence spectral data were collected using a Horiba Jobin Yvon Fluorolog spectrometer. Cyclic voltammetry measurements were performed using a CHI 6205 instrument with a three-electrode setup: Ag/AgCl as a reference electrode, glassy carbon as the working electrode, and Pt wire as the counter electrode. A supporting electrolyte of 0.1 M tetraethyl ammonium perchlorate was utilised, and the complexes were dissolved at a concentration of 0.5 mM in CH_3CN at 298 K. All experiments were conducted under an inert atmosphere. Ferrocene was used as an internal standard, and potentials were adjusted relative to the Ag/AgCl reference electrode ($E_{1/2}$ of +0.197 V).[36]

4.3. Theoretical calculations

Geometry optimizations of the cationic complexes $\mathbf{1}^+$, $\mathbf{2}^+$, and $\mathbf{3}^{2+}$ were carried out using density functional theory (DFT) using the Gaussian 16 software package, in the gas phase.[49] The ground-state geometries were further investigated by time-dependent DFT (TD-DFT) employing the Becke three-parameter hybrid exchange functional in conjunction with the Lee–Yang–Parr correlation functional (B3LYP).[50–52] Harmonic vibrational frequency calculations were performed to confirm that all optimised structures corresponded to global minima on the potential energy surface. The LANL2DZ effective core potential basis set was applied to ruthenium atoms, while the 6-31G(d) basis set was employed for all lighter atoms. A self-consistent field (SCF) convergence criterion of 10^{-10} was used throughout, along with Gaussian's ultrafine pruned integration grid for numerical computations. Molecular orbital (MO) energies and the percentage contributions from individual atomic groups were analysed using the GaussSum 3.0 program.[53]

4.4. Synthetic procedures

The complexes 1–**3** were synthesized by following the procedure described below (Scheme 1).

4.1.1. Synthesis of [(tpy)Ru(phpy)Cl]ClO_4 [1]. A 1 : 1 molar ratio of $[Ru(tpy)Cl_3]$ precursor (50 mg, 0.1 mmol) and **phpy** ligand (43 mg, 0.11 mmol) along with five equivalents of NEt_3 was refluxed with stirring in 20 mL ethanol under a N_2 atmosphere for 18 h. During the course of the reaction, the initial dark brown colour of the solution changed to dark orange. Next, an excess of $NaClO_4$ was added to the hot reaction mixture. The stirring was continued for another hour. Then the reaction mixture was dried under vacuum and approximately 5 mL distilled water was added to it and kept in a freezer for 4 h. This was then filtered, and the precipitate was washed with copious amounts of cold water and dried in air. The crude product obtained was purified using a neutral alumina column using dichloromethane and acetonitrile (4 : 1) as the eluent, yielding pure **1**. Yield: 42 mg (49%). Molar conductivity (Λ_M/Ω^{-1} cm^2 mol^{-1}) in CH_3CN:63. HRMS [(+)-ESI): m/z 756.0961 (calculated molecular mass for 756.0965]. ^1H NMR (400 MHz, DMSO) δ 10.45 (d, J = 6.5 Hz, 1H), 9.79 (d, J = 9.4 Hz, 1H), 9.22 (d, J = 9.1 Hz, 1H), 8.87 (d, J = 8.1 Hz, 2H), 8.71 (d, J = 8.1 Hz, 2H), 8.58 (dd, J = 8.2, 5.4 Hz, 1H), 8.37 (d, J = 4.3 Hz, 1H), 8.33 (t, J = 5.9 Hz, 2H), 8.28 (t, J = 8.1 Hz, 1H), 8.17 (d, J = 7.9 Hz, 1H), 8.10 (t, J = 7.7 Hz, 1H), 8.02 (d, J = 9.3 Hz, 1H), 7.96 (t, J = 8.0 Hz, 2H), 7.90 (d, J = 5.4 Hz, 1H), 7.63 (d, J = 5.2 Hz, 2H), 7.58 (dd, J = 8.1, 5.5 Hz, 1H), 7.47 (dd, J = 7.1, 5.3 Hz, 1H), 7.42 (dd, J = 7.0, 5.3 Hz, 1H), 7.26 (t, J = 6.5 Hz, 2H). ^{13}C NMR (101 MHz, DMSO) δ 158.85, 158.17, 156.82, 156.74, 154.50, 154.34, 153.27, 153.07, 152.95, 151.38, 149.43, 148.91, 148.86, 138.19, 137.71, 137.64, 137.56, 134.69, 132.39, 131.28, 129.37, 128.84, 127.76, 127.38, 126.72, 124.82, 124.73, 124.41, 124.33, 124.19, 123.24.

4.1.2. Synthesis of [(p-cym)Ru(phpy)Cl]ClO_4 [2]. In a round-bottomed flask, 50 mg (0.08 mmol) dimeric $[(p\text{-cym})Ru(\mu\text{-}Cl)Cl]_2$ was taken in 20 mL ethanol. To this, 66 mg (0.2 mmol) **phpy** ligand was added and refluxed with stirring for 12 h under a dinitrogen environment. After completion, an excess of $NaClO_4$ was added to the hot solution and stirred for an additional 1 h, which resulted in a brown coloured precipitate. The reaction mixture was then kept in the freezer for 4 h. This was filtered and the precipitate was then washed with cold water and ethanol and dried in air. The pure **2** was obtained by repeated precipitation using CH_2Cl_2/hexane. Yield: 90 mg (73%). Molar conductivity (Λ_M/Ω^{-1} cm^2 mol^{-1}) in CH_3CN:45. HRMS ((+)-ESI): m/z 657.1086 (calculated molecular mass for 657.0887). ^1H NMR (400 MHz, DMSO) δ 10.06 (d, J = 5.1 Hz, 1H), 9.72 (d, J = 8.2 Hz, 1H), 8.37 (d, J = 4.5 Hz, 1H), 8.34–8.31 (m, 1H), 8.26 (d, J = 7.8 Hz, 1H), 8.07 (t, J = 7.7 Hz, 1H), 7.46 (dd, J = 7.1, 5.3 Hz, 1H), 6.41 (d, J = 6.3 Hz, 1H), 6.18 (d, J = 6.3 Hz, 1H), 2.68 (dt, J = 10.3, 6.1 Hz, 1H), 2.22 (s, 1H), 0.97 (d, J = 6.9 Hz, 3H). ^{13}C NMR (101 MHz, DMSO) δ 157.46, 156.11, 156.08, 153.15, 152.98, 152.94, 148.40, 147.08, 137.30, 136.65, 135.42, 128.55, 127.53, 124.46, 124.07, 104.64, 102.95, 86.04, 84.14, 30.50, 21.78, 18.32.

4.1.3. Synthesis of [(tpy)RuCl(μ-phpy)Ru(p-cym)Cl]$(ClO_4)_2$ [3]. A 2 : 1 molar ratio of mononuclear **1** (55 mg, 0.066 mmol) and $[(p\text{-cym})Ru(\mu\text{-}Cl)Cl]_2$ precursor (20 mg, 0.033 mmol) in 20 mL ethanol was refluxed under a N_2 atmosphere for 12 h. After completion, to the hot solution an excess of $NaClO_4$ was added and stirred for an additional 1 h. The precipitate thus obtained was then filtered and dried. The purple-coloured crude product was then purified using repeated precipitation using CH_3OH/diethyl ether. Yield: 64 mg (79%). Molar conductivity (Λ_M/Ω^{-1} cm^2 mol^{-1}) in CH_3CN: 105. HRMS ((+)-ESI): m/z 1126.0202 (calculated molecular mass for 1126.0277).

^{1}H NMR (400 MHz, DMSO) δ 10.55 (d, J = 5.4 Hz, 1H), 9.82 (d, J = 9.1 Hz, 1H), 9.39 (d, J = 5.7 Hz, 1H), 9.35 (d, J = 5.5 Hz, 1H), 9.25 (d, J = 8.0 Hz, 1H), 8.91 (dd, J = 7.9, 5.8 Hz, 2H), 8.76 (t, J = 9.1 Hz, 2H), 8.68 (dd, J = 8.2, 5.4 Hz, 1H), 8.43 (t, J = 7.7 Hz, 1H), 8.33 (t, J = 8.1 Hz, 2H), 8.25 (d, J = 7.7 Hz, 1H), 8.13 (d, J = 7.1 Hz, 1H), 8.00 (t, J = 6.4 Hz, 3H), 7.92 (t, J = 6.7 Hz, 1H), 7.86 (t, J = 6.7 Hz, 1H), 7.80 (d, J = 5.3 Hz, 1H), 7.68 (dd, J = 8.1, 5.5 Hz, 1H), 7.56 (d, J = 5.2 Hz, 1H), 7.36 (t, J = 6.6 Hz, 1H), 7.29 (t, J = 6.5 Hz, 1H), 5.70 (dd, J = 17.2, 6.0 Hz, 2H), 4.95 (dd, J = 23.8, 6.0 Hz, 2H), 1.61 (s, 3H), 1.06 (dd, J = 11.9, 6.9 Hz, 6H). ^{13}C NMR (101 MHz, DMSO) δ 159.63, 158.83, 158.05, 156.83, 156.75, 155.30, 155.09, 153.27, 153.13, 152.96, 152.62, 151.94, 151.36, 150.97, 150.80, 150.74, 149.94, 149.48, 148.91, 148.86, 141.36, 141.22, 141.17, 139.67, 139.43, 137.81, 137.75, 134.91, 132.98, 131.91, 130.38, 130.31, 129.39, 129.29, 129.08, 128.84, 127.87, 127.78, 127.17, 127.02, 124.83, 124.75, 124.35, 124.30, 123.44, 123.37, 102.76, 102.24, 88.16, 88.05, 82.41, 30.46, 22.28, 17.66.

Author contributions

Ms Anwesha Mohanty: data collection, analysis and/or interpretation of the data, drafting and revising the manuscript. Dr Srikanta Patra: conceptualization, analysis and/or interpretation of the data, drafting and revising the original manuscript, funding acquisition, project supervision.

Conflicts of interest

There are no conflicts to declare.

Abbreviations

s	Singlet
d	Doublet
t	Triplet
m	Multiplet
dd	Doublet of doublet
CT-DNA	Calf thymus DNA

Data availability

The data supporting this article have been included as part of the ESI.†

Acknowledgements

This work was partially supported by the SERB, DST (CRG/2018/000173), New Delhi, and CSIR (No. 01(2932)/18/EMR-II dated 01/05/2018), New Delhi. AM is thankful to UGC, New Delhi, India, for the fellowship.

References

1 M. N. Dunbar, S. J. Steinke, E. J. Piechota and C. Turro, *J. Phys. Chem. A*, 2024, **128**, 599–610.
2 A. Juris, V. Balzani, F. Barigelletti, S. Campagna, P. Belser and A. von Zelewsky, *Coord. Chem. Rev.*, 1988, **84**, 85–277.
3 L. Hammarström, *Acc. Chem. Res.*, 2015, **48**, 840–850.
4 M. T. Rupp, N. Shevchenko, G. S. Hanan and D. G. Kurth, *Coord. Chem. Rev.*, 2021, **446**, 214127.
5 C. A. Puckett and J. K. Barton, *J. Am. Chem. Soc.*, 2007, **129**, 46–47.
6 O. Nováková, J. Kašpárková, O. Vrána, P. M. van Vliet, J. Reedijk and V. Brabec, *Biochemistry*, 1995, **34**, 12369–12378.
7 A. M. Pyle, J. P. Rehmann, R. Meshoyrer, N. J. Turro, J. K. Barton and C. V. Kumar, *J. Am. Chem. Soc.*, 1989, **111**, 3051–3058.
8 A. E. Friedman, J. K. Barton, J. C. Chambron, J. P. Sauvage and N. J. Turro, *J. Am. Chem. Soc.*, 1990, **112**, 4960–4962.
9 C. S. Allardyce and P. J. Dyson, *Platinum Met. Rev.*, 2001, **45**, 62–69.
10 Y. Lu, Z. Hou, M. Li, N. Wang, J. Wang, F. Ni, Y. Zhao, B. Zhang and N. Xi, *Dalton Trans.*, 2022, **51**, 16224–16235.
11 Y. Lu, A. F. M. Motiur Rahman and Y. Jahng, *Arch. Pharmacal Res.*, 2017, **40**, 563–570.
12 M. Dutta, K. K. Bania and S. Pratihar, *Chem. – Asian J.*, 2020, **15**, 926–932.
13 R. Colaiezzi, C. Saviozzi, N. di Nicola, S. Zacchini, G. Pampaloni, M. Crucianelli, F. Marchetti, A. Di Giuseppe and L. Biancalana, *Catal. Sci. Technol.*, 2023, **13**, 2160–2183.
14 S. Yadav and R. Gupta, *ACS Sustainable Chem. Eng.*, 2023, **11**, 8533–8543.
15 C. Pettinari, F. Marchetti, A. Cerquetella, R. Pettinari, M. Monari, T. C. O. Mac Leod, L. M. D. R. S. Martins and A. J. L. Pombeiro, *Organometallics*, 2011, **30**, 1616–1626.
16 C. G. Hartinger and P. J. Dyson, *Chem. Soc. Rev.*, 2009, **38**, 391–401.
17 S. K. Tripathy, R. K. Surada, R. K. Manne, S. M. Mobin, M. K. Santra and S. Patra, *Dalton Trans.*, 2013, **42**, 14081–14091.
18 G. E. Giacomazzo, L. Conti, C. Fagorzi, M. Pagliai, C. Andreini, A. Guerri, B. Perito, A. Mengoni, B. Valtancoli and C. Giorgi, *Inorg. Chem.*, 2023, **62**, 7716–7727.
19 D. Ossipov, S. Gohil and J. Chattopadhyaya, *J. Am. Chem. Soc.*, 2002, **124**, 13416–13433.
20 L. N. Lameijer, T. G. Brevé, V. H. S. van Rixel, S. H. C. Askes, M. A. Siegler and S. Bonnet, *Chem. – Eur. J.*, 2018, **24**, 2709–2717.
21 H. Chen, J. A. Parkinson, R. E. Morris and P. J. Sadler, *J. Am. Chem. Soc.*, 2003, **125**, 173–186.
22 T. Singh, A. Mary, T. Gupta, P. Sharma, V. Kumar, A. D. Jose and A. R. Naziruddin, *Dalton Trans.*, 2025, **54**, 6517–6528.
23 Y. Cheret, A. Szukalski, K. A. Haupa, A. Popczyk, J. Mysliwiec, B. Sahraoui and A. El-Ghayoury, *Polyhedron*, 2023, **233**, 116299.
24 J. P. Sauvage, J. P. Collin, J. C. Chambron, S. Guillerez, C. Coudret, V. Balzani, F. Barigelletti, L. De Cola and L. Flamigni, *Chem. Rev.*, 1994, **94**, 993–1019.

25 K. S. Joya and H. J. M. De Groot, *Int. J. Hydrogen. Energy*, 2012, **37**, 8787–8799.
26 J. Mola, E. Mas-Marza, X. Sala, I. Romero, M. Rodríguez, C. Viñas, T. Parella and A. Llobet, *Angew. Chem., Int. Ed.*, 2008, **47**, 5830–5832.
27 L. C. C. Lee and K. K. W. Lo, *Chem. Rev.*, 2024, **124**, 8825–9014.
28 T. Ganguly, S. Das, D. Maity and S. Baitalik, *Inorg. Chem.*, 2024, **63**, 6883–6897.
29 Q. X. Zhou, F. Yang, W. H. Lei, J. R. Chen, C. Li, Y. J. Hou, X. C. Ai, J. P. Zhang, X. S. Wang and B. W. Zhang, *J. Phys. Chem. B*, 2009, **113**, 11521–11526.
30 M. W. Cooke, G. S. Hanan, F. Loiseau, S. Campagna, M. Watanabe and Y. Tanaka, *J. Am. Chem. Soc.*, 2007, **129**, 10479–10488.
31 R. Kaur, B. Singh, V. Singh, M. Zharnikov and P. Chandra Mondal, *Coord. Chem. Rev.*, 2024, **514**, 215872.
32 K. Heinze, K. Hempel and M. Beckmann, *Eur. J. Inorg. Chem.*, 2006, 2040–2050.
33 Y. C. Dai, W. Yang, X. Chen, L. H. Gao and K. Z. Wang, *Electrochim. Acta*, 2014, **134**, 319–326.
34 D. G. Brown, N. Sanguantrakun, B. Schulze, U. S. Schubert and C. P. Berlinguette, *J. Am. Chem. Soc.*, 2012, **134**, 12354–12357.
35 S. K. Tripathy, U. De, N. Dehury, S. Pal, H. S. Kim and S. Patra, *Dalton Trans.*, 2014, **43**, 14546–14549.
36 S. Mishra, S. Tripathy, D. Paul, P. Laha, M. Santra and S. Patra, *Inorg. Chem.*, 2023, **62**, 7003–7013.
37 S. Patra, B. Sarkar, S. Ghumaan, M. P. Patil, S. M. Mobin, R. B. Sunoj, W. Kaim and G. K. Lahiri, *Dalton Trans.*, 2005, 1188–1194.
38 Q. X. Zhou, F. Yang, W. H. Lei, J. R. Chen, C. Li, Y. J. Hou, X. C. Ai, J. P. Zhang, X. S. Wang and B. W. Zhang, *J. Phys. Chem. B*, 2009, **113**, 11521–11526.
39 L. Biancalana, L. K. Batchelor, T. Funaioli, S. Zacchini, M. Bortoluzzi, G. Pampaloni, P. J. Dyson and F. Marchetti, *Inorg. Chem.*, 2018, **57**, 6669–6685.
40 N. Chanda, S. M. Mobin, V. G. Puranik, A. Datta, M. Niemeyer and G. K. Lahiri, *Inorg. Chem.*, 2004, **43**, 1056–1064.
41 D. Lazić, A. Arsenijević, R. Puchta, Ž. D. Bugarčić and A. Rilak, *Dalton Trans.*, 2016, **45**, 4633–4646.
42 F. M. S. de Alencar, F. S. Gouveia, G. de, F. S. de Oliveira, A. L. Andrade, M. A. de Vasconcelos, A. P. Ayala, A. C. S. Gondim, I. M. M. de Carvalho, C. A. F. Moraes, M. V. Palmeira-Mello, A. A. Batista, L. G. de, F. Lopes and E. H. S. Sousa, *Dalton Trans.*, 2025, **54**, 1850–1870.
43 S. De, R. Selva Kumar, A. Gauthaman, S. K. Ashok Kumar, P. Paira, A. Moorthy and S. Banerjee, *Inorg. Chim. Acta*, 2021, **515**, 120066.
44 M. M. Milutinović, A. Rilak, I. Bratsos, O. Klisurić, M. Vraneš, N. Gligorijević, S. Radulović and Ž. D. Bugarčić, *J. Inorg. Biochem.*, 2017, **169**, 1–12.
45 N. Kumar, R. Kaushal and P. Awasthi, *J. Mol. Struct.*, 2023, **1288**, 135751.
46 O. Novakova, H. Chen, O. Vrana, A. Rodger, P. J. Sadler and V. Brabec, *Biochemistry*, 2003, **42**, 11544–11554.
47 B. P. Sullivan, J. M. Calvert and T. J. Meyer, *Inorg. Chem.*, 1980, **19**, 1404–1407.
48 M. A. Bennett, T.-N. Huang and T. W. Matheson, *Inorg. Synth.*, 1982, **21**, 74–78.
49 G. E. S. M. J. Frisch, G. W. Trucks, H. B. Schlegel, V. B. M. A. Robb, J. R. Cheeseman, G. Scalmani, M. C. B. Mennucci, G. A. Petersson, H. Nakatsuji, G. Z. X. Li, H. P. Hratchian, A. F. Izmaylov, J. Bloino, R. F. J. L. Sonnenberg, M. Hada, M. Ehara, K. Toyota, O. K. J. Hasegawa, M. Ishida, T. Nakajima, Y. Honda, J. E. P. H. Nakai, T. Vreven, J. A. MontgomeryJr., E. N. B. F. Ogliaro, M. J. Bearpark, J. Heyd, J. N. K. N. Kudin, V. N. Staroverov, R. Kobayashi, S. S. I. K. Raghavachari, A. P. Rendell, J. C. Burant, M. K. J. Tomasi, M. Cossi, N. Rega, N. J. Millam, J. J. J. E. Knox, J. B. Cross, V. Bakken, C. Adamo, A. J. A. R. Gomperts, R. E. Stratmann, O. Yazyev, R. L. M. R. Cammi, C. Pomelli, J. W. Ochterski, P. S. K. Morokuma, V. G. Zakrzewski, G. A. Voth, Ö. F. J. J. Dannenberg, S. Dapprich, A. D. Daniels, G. J. B. Foresman, J. V. Ortiz, J. Cioslowski and D. J. Fox, *W. 09, revision A.1*, Gaussian Inc., Gaussian, Inc., Wallingford CT, 2009, preprint.
50 A. D. Becke, *J. Chem. Phys.*, 1993, **98**, 5648–5652.
51 C. Lee, W. Yang and R. G. Parr, *Phys. Rev. B:Condens. Matter Mater. Phys.*, 1988, **37**, 785.
52 S. H. Vosko, L. Wilk and M. Nusair, *Can. J. Phys.*, 1980, **58**, 1200–1211.
53 N. M. O'Boyle, A. L. Tenderholt and K. M. Langner, *J. Comput. Chem.*, 2008, **29**, 839–845.